nature materials

LETTERS

PUBLISHED ONLINE: 14 DECEMBER 2008 | DOI: 10.1038/NMAT2342

Tunable magnetic exchange interactions in manganese-doped inverted core–shell ZnSe–CdSe nanocrystals

David A. Bussian[1,2], Scott A. Crooker[3]*, Ming Yin[1], Marcin Brynda[4], Alexander L. Efros[5] and Victor I. Klimov[1,2]*

Magnetic doping of semiconductor nanostructures is actively pursued for applications in magnetic memory and spin-based electronics[1,2]. Central to these efforts is a drive to control the interaction strength between carriers (electrons and holes) and the embedded magnetic atoms[3–5]. In this respect, colloidal nanocrystal heterostructures provide great flexibility through growth-controlled 'engineering' of electron and hole wavefunctions in individual nanocrystals[6,7]. Here, we demonstrate a widely tunable magnetic *sp–d* exchange interaction between electron–hole excitations (excitons) and paramagnetic manganese ions using 'inverted' core–shell nanocrystals composed of Mn^{2+}-doped ZnSe cores overcoated with undoped shells of narrower-gap CdSe. Magnetic circular dichroism studies reveal giant Zeeman spin splittings of the band-edge exciton that, surprisingly, are tunable in both magnitude and sign. Effective exciton *g*-factors are controllably tuned from −200 to +30 solely by increasing the CdSe shell thickness, demonstrating that strong quantum confinement and wavefunction engineering in heterostructured nanocrystal materials can be used to manipulate carrier–Mn^{2+} wavefunction overlap and the *sp–d* exchange parameters themselves.

Traditionally, embedding paramagnetic atoms into low-dimensional semiconductor structures requires molecular-beam epitaxy or chemical vapour deposition techniques[3–5]. There now exists a rich variety of 'diluted magnetic semiconductor' (DMS) quantum wells, superlattices and hetero-interfaces, with recent work demonstrating magnetic doping of epitaxially grown 'zero-dimensional' quantum dots[8–10]. In parallel, advances in colloidal chemistry have recently enabled magnetic doping of semiconductor nanocrystals[11–16], providing an alternative and potentially lower-cost route towards magnetically active quantum dots. With a view towards enhancing carrier/paramagnetic ion spin interactions, colloidal nanocrystals typically generate stronger spatial confinement of electronic wavefunctions compared with their epitaxial counterparts, which is thought to enhance *sp–d* exchange coupling even for a single magnetic dopant atom[12,17].

Whereas magnetically doped monocomponent nanocrystals are well established[16], wavefunction engineering using magnetic multicomponent colloidal heterostructures[18,19] has not been extensively explored. One new class of nanocrystal heterostructure that holds promise for tuning *sp–d* exchange interactions are 'inverted' core–shell designs, wherein wide-gap semiconductor cores are overcoated with narrower-gap shells. With increasing shell thickness, the electron and hole envelope wavefunctions, $\Psi_{e,h}(\mathbf{r})$, migrate towards the nanocrystal periphery[7] (albeit at different rates), thus tuning their overlap with magnetic atoms embedded, for example, in the core alone. Here, we investigate precisely this type of wavefunction engineering and exchange interaction control using 'inverted' ZnSe–CdSe core–shell nanocrystals in which the cores are doped with paramagnetic, spin-5/2 Mn^{2+} ions (see Fig. 1). Magnetic circular dichroism (MCD) spectroscopy at the nanocrystal absorption edge reveals a giant *sp–d* exchange interaction that inverts sign with increasing shell thickness, suggesting a confinement-induced sign inversion of the electron–Mn^{2+} exchange constant, α, accompanied by significant reduction of the hole–Mn^{2+} overlap due to wavefunction engineering.

Four series of ZnSe–CdSe nanocrystals were grown, each having ZnSe cores of radius $r \cong 17$ Å. In each series the CdSe shell thickness, h, systematically increases from 0 to 8 Å. Two series used non-magnetic (undoped) 'reference' cores, and two used Mn^{2+}-doped cores. Elemental analysis of pyridine-washed magnetic cores indicates ~2 Mn^{2+} ions per core, on average. Paramagnetic resonance studies are consistent with the Mn^{2+} residing primarily in the ZnSe core, for all h (see Supplementary Information). Figure 1a shows absorption and photoluminescence spectra from the Mn^{2+}-doped ZnSe cores alone ($h = 0$). The absorption peak at ~3.2 eV is due to the fundamental band-edge (1S) exciton transition. On the other hand, the photoluminescence is dominated by the 2.15 eV internal $^4T_1 \rightarrow {}^6A_1$ Mn^{2+} transition, which results from efficient energy transfer from band-edge excitons to the excited $^4T_1$ Mn^{2+} state[11]. The photoluminescence also shows a small peak at 2.95 eV from direct recombination of band-edge excitons[14,19].

To suppress energy transfer and realize strong exciton photoluminescence, the nanocrystal bandgap must be tuned below ~2.15 eV, as recently demonstrated in Mn^{2+}-doped CdSe nanocrystals (ref. 20). This regime is accessible here using sufficiently thick shells (see Fig. 1b). Increasing h shifts $\Psi_e(\mathbf{r})$ and $\Psi_h(\mathbf{r})$ towards the shell, reducing the bandgap and redshifting both the absorption and the photoluminescence. When $h \geqslant 5$ Å, the exciton photoluminescence energy drops below 2.15 eV. The dependence of the exciton photoluminescence energy on the absorption energy is summarized in Fig. 1c, for both Mn^{2+}-doped and non-magnetic nanocrystals.

[1]Chemistry Division, Los Alamos National Laboratory, Los Alamos, New Mexico 87545, USA, [2]Center for Integrated Nanotechnologies, Los Alamos, New Mexico 87545, USA, [3]National High Magnetic Field Laboratory, Los Alamos, New Mexico 87545, USA, [4]Department of Chemistry, University of California, Davis, California 95616, USA, [5]Naval Research Laboratory, Washington, District of Columbia 20375, USA. *e-mail: crooker@lanl.gov; klimov@lanl.gov.

Report Documentation Page

Form Approved
OMB No. 0704-0188

1. REPORT DATE	2. REPORT TYPE	3. DATES COVERED
JAN 2009		**00-00-2009 to 00-00-2009**

4. TITLE AND SUBTITLE	5a. CONTRACT NUMBER
Tunable magnetic exchange interactions in manganese-doped inverted core-shell ZnSe-CdSe nanocrystals	5b. GRANT NUMBER
	5c. PROGRAM ELEMENT NUMBER
6. AUTHOR(S)	5d. PROJECT NUMBER
	5e. TASK NUMBER
	5f. WORK UNIT NUMBER
7. PERFORMING ORGANIZATION NAME(S) AND ADDRESS(ES) **Naval Research Laboratory,Washington,DC,20375**	8. PERFORMING ORGANIZATION REPORT NUMBER
9. SPONSORING/MONITORING AGENCY NAME(S) AND ADDRESS(ES)	10. SPONSOR/MONITOR'S ACRONYM(S)
	11. SPONSOR/MONITOR'S REPORT NUMBER(S)

12. DISTRIBUTION/AVAILABILITY STATEMENT
Approved for public release; distribution unlimited

13. SUPPLEMENTARY NOTES

14. ABSTRACT

15. SUBJECT TERMS

16. SECURITY CLASSIFICATION OF:			17. LIMITATION OF ABSTRACT	18. NUMBER OF PAGES	19a. NAME OF RESPONSIBLE PERSON
a. REPORT **unclassified**	b. ABSTRACT **unclassified**	c. THIS PAGE **unclassified**	**Same as Report (SAR)**	**6**	

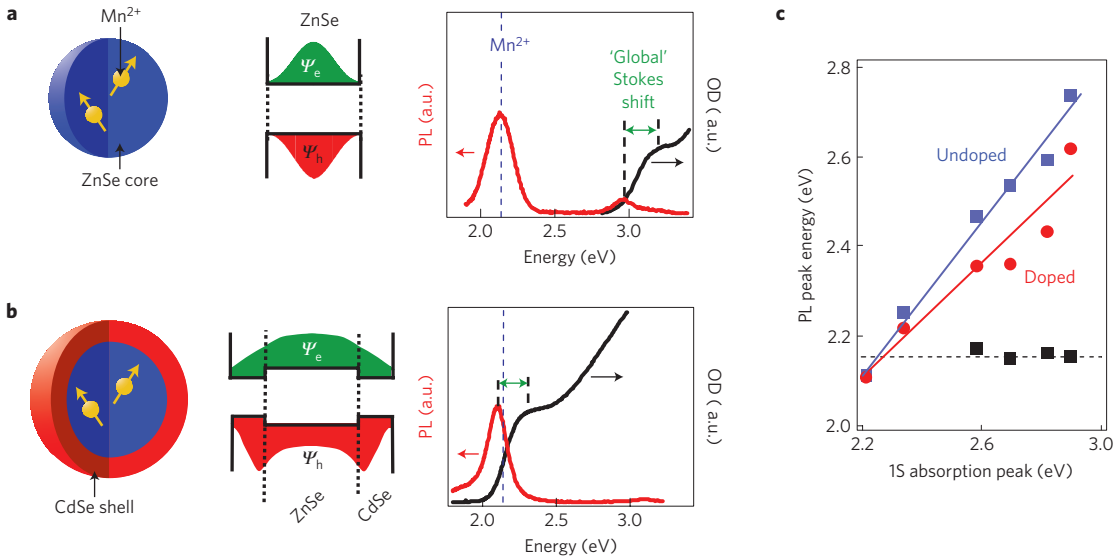

Figure 1 | An 'inverted core–shell' approach to tuning *sp–d* spin-exchange interactions in heterostructured colloidal nanocrystals. a,**b**, Mn^{2+}-doped cores of wide-bandgap ZnSe are overcoated with narrower-gap CdSe shells of increasing thickness *h*. The conduction and valence band diagrams show the notional electron and hole wavefunctions in these nanocrystals. Room-temperature photoluminescence (PL) and absorption spectra (OD: optical density) from representative solutions of Mn^{2+}-doped ZnSe cores alone (**a**) and Mn^{2+}-doped cores with thick ($h \sim 8$ Å) CdSe shells (**b**). With increasing *h*, the band-edge photoluminescence energy approaches and drops below the internal Mn^{2+} $^4T_1 \rightarrow {}^6A_1$ emission at ~2.15 eV. **c**, Dependence of the band-edge exciton photoluminescence energy on the 1S absorption peak energy. Red symbols show nanocrystals with Mn^{2+}-doped cores, and blue symbols show nanocrystals with non-magnetic 'reference' cores. The Mn^{2+} emission at ~2.15 eV is shown by black squares.

The most compelling evidence for successful Mn^{2+} incorporation is an enhanced exciton Zeeman splitting, ΔE_Z, due to carrier–Mn^{2+} *sp–d* exchange. Low-temperature MCD spectroscopy provides a direct, quantitative measure of ΔE_Z at the fundamental 1S absorption peak[21]. Figure 2 shows ΔE_Z versus magnetic field **H** at different temperatures for four important cases: non-magnetic and Mn^{2+}-doped ZnSe–CdSe nanocrystals, each having 'thin' and 'thick' shells. Non-magnetic nanocrystals with thin or thick shells show MCD signals that track the derivative of the absorption peak and increase linearly with field from 1–6 T (Fig. 2a,b, insets). The exciton Zeeman splittings, $\Delta E_Z = g_{ex}\mu_B\mathbf{H}$, where μ_B is the Bohr magneton, indicate small, temperature-independent, positive exciton *g*-factors of order unity ($g_{ex} = +2.1$ and $+2.5$, respectively), in approximate agreement with previous studies of non-magnetic monocomponent nanocrystals (refs 14,21). As expected, shell thickness does not strongly influence the small intrinsic electron and hole *g*-factors in these non-magnetic nanocrystals.

Magnetic nanocrystals having thin shells (Fig. 2c) exhibit much larger MCD of opposite sign. ΔE_Z is negative, quite large, and tracks the temperature-dependent magnetization of the paramagnetic Mn^{2+} ions, which is described by a Brillouin function (dashed line). These data reveal a strong *sp–d* exchange interaction between the absorption-edge exciton and the Mn^{2+} in the ZnSe core, and are qualitatively similar to previous studies[12,14,15] of monocomponent ZnSe or CdSe nanocrystals doped with Mn^{2+} or Co^{2+}.

In surprising contrast, Fig. 2d reveals that in Mn^{2+}-doped nanocrystals with thick CdSe shells, ΔE_Z has opposite sign, yet still exhibits a significant *sp–d* coupling: ΔE_Z still saturates at low temperatures and high fields and is significantly larger than in non-magnetic nanocrystals. Carrier–Mn^{2+} *sp–d* exchange coupling is clearly still appreciable; however, its sign has inverted. A clear inversion of the *sp–d* exchange is seen in Fig. 3a, which shows ΔE_Z versus **H** at 1.6 K for one series of Mn^{2+}-doped ZnSe–CdSe nanocrystals. In this series, the 1S absorption edge drops from 2.9 eV (red trace) to 2.2 eV (purple trace) as *h* increases to 8 Å. For all nanocrystals in this magnetic series, ΔE_Z exhibits saturation at high magnetic fields (and also reveals a Brillouin-function temperature dependence; not shown), indicating significant *sp–d* interactions. ΔE_Z inverts when $h \sim 2$ Å. For comparison, the small, linear ΔE_Z from non-magnetic nanocrystals is also shown (black trace). Effective exciton *g*-factors derived from the low-field Zeeman splitting, g_{eff}, along with g_{eff} from all other nanocrystal series, are plotted in Fig. 3b versus the absorption energy. With increasing *h*, g_{eff} is tuned from -200 to $+30$.

Although elegant experiments in DMS quantum wells have shown that the net *sp–d* interaction's magnitude is tunable through wavefunction engineering[22], to our knowledge its sign has never been shown to invert, which is unexpected in the traditional framework of *sp–d* exchange (discussed below) and which points to new physics in these core–shell nanocrystal materials. In the following, we show that the inversion of ΔE_Z can arise, in part, from the strong 'zero-dimensional' quantum confinement realized in nanocrystals, which exceeds that typically found in two-dimensional heterostructures, and which can invert the sign of α, the electron–Mn^{2+} exchange parameter.

Although a single Mn^{2+} spin interacting with a single exciton will generate—even in zero field—a measurable ΔE_Z in a single quantum dot[10,12], our colloidal nanocrystal cores each contain ~2 Mn^{2+} spins on average, in which the overlap-weighted average magnetization determines ΔE_Z in any given nanocrystal. Furthermore, we study ensembles of nanocrystals. The Mn^{2+} in the ZnSe cores are positioned randomly, and the number of Mn^{2+} per core fluctuates statistically, enabling us to discuss *sp–d* exchange interactions in these nanocrystal ensembles in terms of a pseudo-bulk model. Here, spin splittings of the conduction and valence band edges in the nanocrystals have two contributions: (1) a small splitting from the 'intrinsic' electron and hole *g*-factors in the host semiconductor, $g_{e,h}$ (of order unity in CdSe and ZnSe), and (2) a potentially much larger splitting from the *s–d* (*p–d*) exchange interaction between the $\mathbf{s}_e = 1/2$, *s*-like electrons ($\mathbf{j}_h = 3/2$, *p*-like holes) and the $\mathbf{S} = 5/2$ *d*-shell moments of the Mn^{2+}. The *s–d* and *p–d* character of the electron–Mn^{2+} and hole–Mn^{2+} interaction are characterized by the exchange energies $N_0\alpha$ and $N_0\beta$, respectively, where N_0 is the density of unit cells. In bulk II–VI DMSs (refs 3,23),

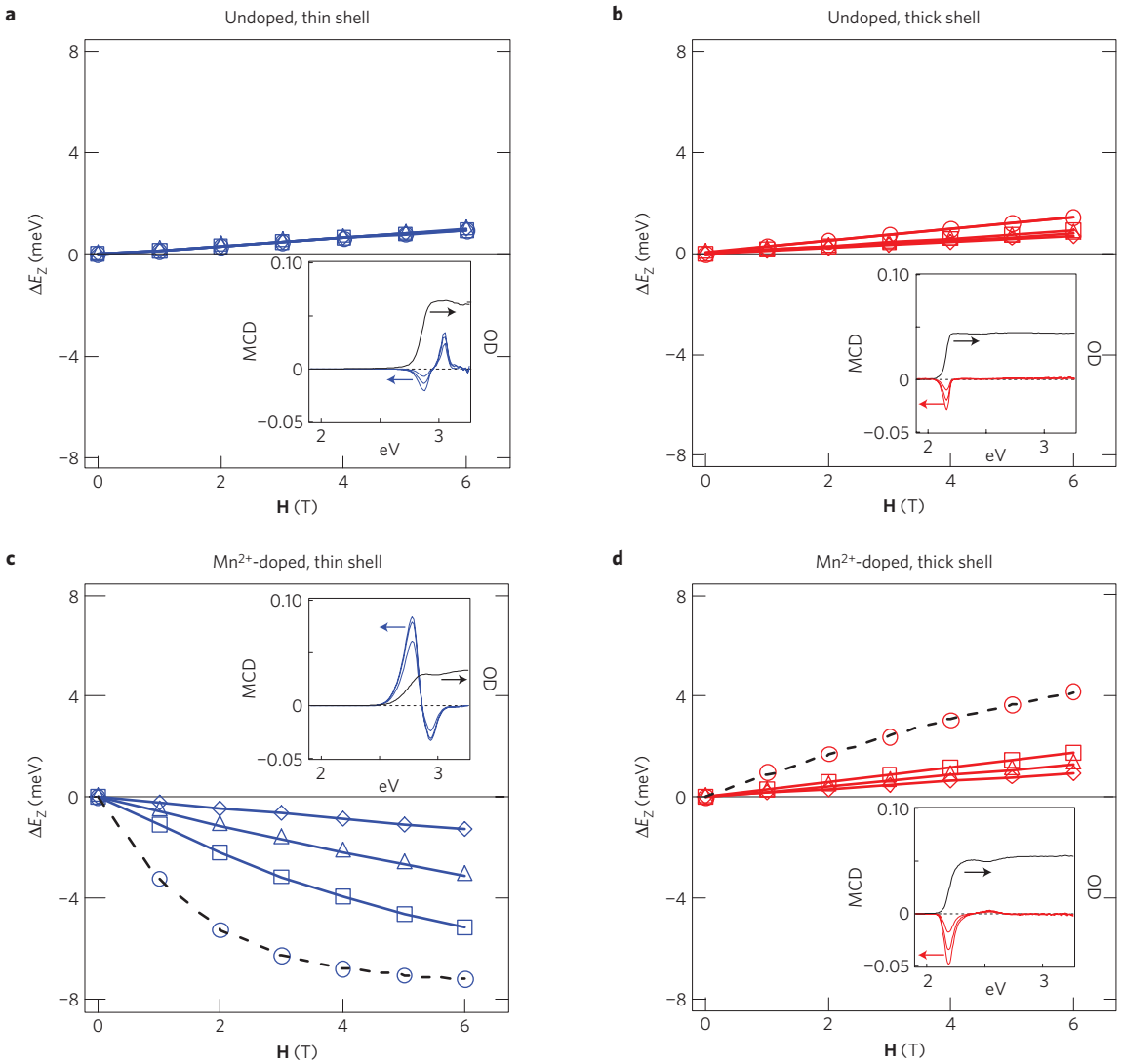

Figure 2 | Magnetic-field- and temperature-dependent Zeeman spin splitting, ΔE_Z, and MCD spectra from both magnetic and non-magnetic core–shell nanocrystals. ΔE_Z versus **H** at the fundamental 1S absorption peak from ZnSe–CdSe nanocrystals at $T = 3$ K (circles), 10 K (squares), 20 K (triangles) and 50 K (diamonds). The insets show absorption and MCD spectra at $T = 3$ K, for $\mathbf{H} = 2$, 4 and 6 T. **a**–**d**, Measurements on nanocrystals having undoped ZnSe cores and thin ($h \sim 1$ Å) CdSe shells (**a**), undoped cores with thick ($h \sim 7$ Å) shells (**b**), Mn^{2+}-doped cores with thin shells (**c**) and Mn^{2+}-doped cores with thick shells (**d**). Note that the MCD and ΔE_Z inverts sign in Mn^{2+}-doped nanocrystals when shell thickness increases (**c**,**d**). The black dashed lines in **c**,**d** show modified Brillouin-function fits to ΔE_Z at $T = 3$ K, using effective temperatures $T + T_0 = 4$ and 9 K, respectively (see the Methods section).

$N_0\alpha$ arises from potential (ferromagnetic) *s*–*d* exchange and is positive, whereas $N_0\beta$ derives predominantly from kinetic-type (antiferromagnetic) *p*–*d* exchange and is larger and negative. In bulk $Zn_{1-x}Mn_xSe$ ($Cd_{1-x}Mn_xSe$), $N_0\alpha = +0.29$ eV (+0.23 eV) and $N_0\beta = -1.4$ eV (−1.27 eV (ref. 23)).

In analogy with bulk DMS materials[3,23], *s*–*d* and *p*–*d* exchange in our core–shell nanocrystals generates a spin splitting between the $s_z = \pm 1/2$ electrons and the $j_z = \pm 3/2$ holes equal to $f_e N_0\alpha\langle S_z\rangle$ and $f_h N_0\beta\langle S_z\rangle$, respectively. In our nanocrystals, f_e and f_h characterize the degree of spatial overlap between the Mn^{2+} ions in the core and the modulus-square of the wavefunctions $\Psi_e(\mathbf{r})$ and $\Psi_h(\mathbf{r})$ (in bulk DMSs, f_e and f_h simply equal the average percentage of Mn^{2+} cations). In an ensemble of nanocrystals, f_e and f_h can therefore be regarded as the average probability that the electron and hole reside in the core, multiplied by the average percentage of Mn^{2+} cations per core. The last quantity, $\langle S_z\rangle$, is the average spin projection per Mn^{2+} along **H**. For low Mn^{2+} doping, $\langle S_z\rangle$ follows a Brillouin function, which describes the magnetization of paramagnetic Mn^{2+} moments; that is, $\langle S_z\rangle$ saturates at low temperatures and high magnetic fields. By convention $\langle S_z\rangle$ is negative, being oriented antiparallel to **H**.

In colloidal II–VI nanocrystals, experiments and theory have established[24] that band-edge, 1S excitons (nominally composed of twofold degenerate $\mathbf{s}_e = 1/2$ electrons and fourfold degenerate $\mathbf{j}_h = 3/2$ holes) are split by the effects of strong electron–hole exchange, crystal field and shape asymmetry into five distinct levels labelled by F, the total angular momentum projection on the nanocrystal symmetry axis: $F = 2$, 1^L, 0^L, 1^U and 0^U, where 'U/L' denotes upper/lower manifold levels. Figure 4a shows the ordering of these levels in nearly spherical nanocrystals. Exciton photoluminescence originates primarily from the lower optically active state (1^L), whereas the band-edge absorption peak derives from the upper 1^U transition, which has much larger oscillator strength. The energy separating the $1^{L,U}$ states gives the large 'global' Stokes shift typically observed in nanocrystals (see Fig. 1). Both 1^U and 1^L excitons are twofold degenerate with respect to total angular momentum ($F = \pm 1^{L,U}$). Thus, the MCD originates in the Zeeman

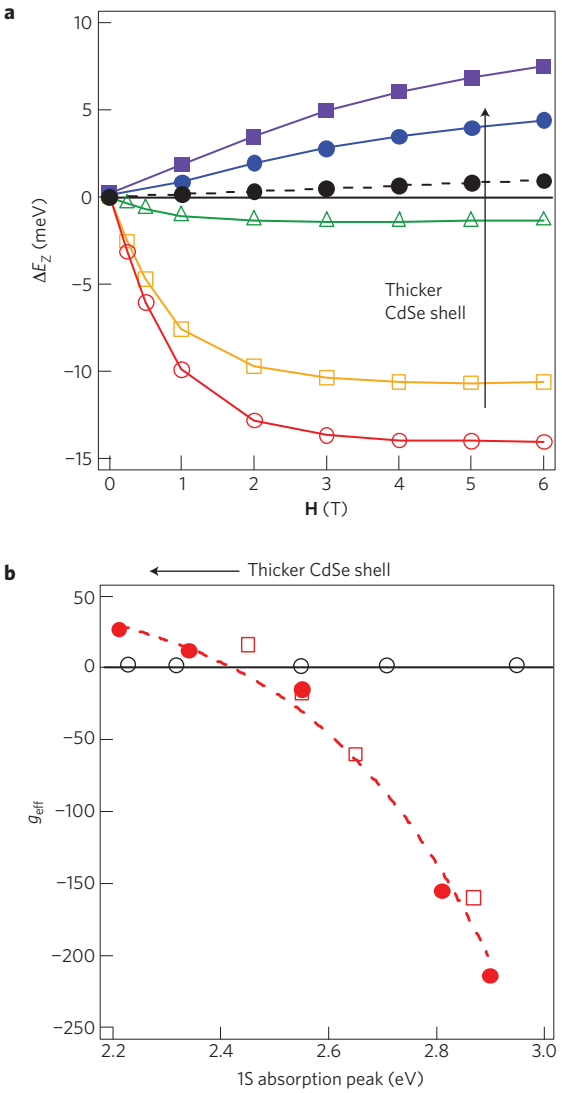

Figure 3 | Field-dependent Zeeman splitting of the 1S absorption peak, ΔE_Z, and corresponding effective exciton *g*-factors at $T = 1.6$ K. a, The measured ΔE_Z for one series of Mn^{2+}-doped ZnSe–CdSe nanocrystals having different CdSe shell thickness h ranging from $h < 1$ Å (red) to $h \sim 8$ Å (purple). The black symbols show ΔE_Z for non-magnetic 'reference' core–shell nanocrystals. **b**, Effective exciton *g*-factors, g_{eff}, derived from the low-field Zeeman splitting at 1.6 K, plotted as a function of the 1S absorption edge energy. Also shown are g_{eff} from the non-magnetic 'reference' core–shell nanocrystals (black symbols). g_{eff} inverts when $h \sim 2$ Å.

spin splitting of the absorbing $\pm 1^U$ states, which couple to $\sigma^{\pm}$ photons respectively.

In our ZnSe cores, the 1^U transition is composed largely (75%) of transitions from $j_z = \pm 3/2$ hole states, with a small (25%) admixture from $j_z = \pm 1/2$ hole transitions[24]. Neglecting the latter contribution and using the standard selection rules for the absorption of circularly polarized light, we can express ΔE_Z measured in these nanocrystal ensembles as:

$$\Delta E_Z = (3g_h - g_e)\mu_B H + \langle S_z \rangle N_0 (f_e \alpha - f_h \beta), \qquad (1)$$

which is very similar to that in conventional DMS materials. Note that in bulk DMSs, where $\alpha > 0$ and $\beta \cong -4\alpha$, the small 'intrinsic' contribution to ΔE_Z (first term; of order $+0.1$ meV T^{-1} in ZnSe) is typically overwhelmed by the large and negative *sp–d* contribution, which can exceed -100 meV at low temperatures and a few tesla.

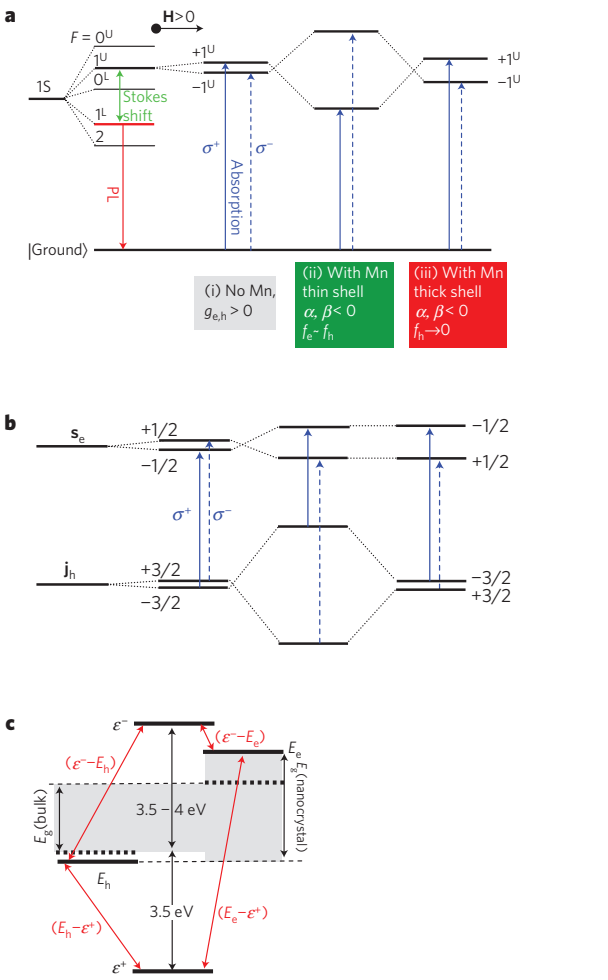

Figure 4 | Energy level diagrams illustrating the Zeeman splitting at the nanocrystal absorption edge, in both an exciton and an electron–hole picture. a, The five exciton levels of the 1S band-edge exciton in nanocrystals. The 1^L and 1^U exciton states are primarily responsible for photoluminescence and absorption, respectively, and their separation gives the 'global' Stokes shift. MCD derives from the Zeeman splitting of the absorbing $\pm 1^U$ states. According to the experimental data, the order of the $+1^U$ and -1^U states changes on introduction of Mn^{2+} ions into nanocrystals with thin shells, but remains unchanged for the case of nanocrystals with thick shells. In both cases, however, the Zeeman splitting in doped nanocrystals greatly exceeds that in undoped nanocrystals. **b**, Representation of the Zeeman splitting of the 1^U excitonic state in terms of the individual splittings of the $s_z = \pm 1/2$ electron and $j_z = \pm 3/2$ hole states that comprise the 1^U exciton, for the case of (i) non-magnetic nanocrystals, (ii) Mn^{2+}-doped nanocrystals with thin CdSe shells and (iii) Mn^{2+}-doped nanocrystals with thick CdSe shells. Independent of shell thickness, introduction of Mn^{2+} ions into nanocrystals changes the order of the $+1/2$ and $-1/2$ electron states, assuming that the sign of α is inverted in nanocrystals compared with the bulk. For thin shells, however, the 'excitonic' exchange is still dominated by hole–Mn^{2+} interactions; therefore, the resulting Zeeman splitting observed in MCD is qualitatively similar to that in bulk DMS materials. Alternatively, for thick shells the strength of the Mn^{2+}–hole interaction is decreased because holes become primarily shell-localized. As a result, the measured excitonic splitting is dominated by the 'sign-inverted' electron–Mn^{2+} interaction. **c**, A diagram showing the relative energies of quantum-confined electron and hole levels in the nanocrystal (E_e and E_h) and the occupied and unoccupied Mn 3*d* levels (ε^+ and ε^-). Red arrows show the virtual transitions that enter into calculations of the confinement-induced contribution of kinetic exchange to α (described in the text).

Equation (1) provides a good description of the average ΔE_Z in these ensembles of Mn^{2+}-doped nanocrystals, and hence the observed inversion of ΔE_Z for $h > \sim 2$ Å indicates a sign reversal of the average exchange term, $(f_e\alpha - f_h\beta)$. Clearly, simply modifying the overlap integrals $f_{e,h}$ by wavefunction engineering cannot invert this quantity if α and β retain the same sign as in the bulk (positive and negative, respectively). Rather, the sign of α or β in these nanocrystals must be different than in the bulk. Such a possibility is indeed expected on the basis of recent experiments in DMS quantum wells[25–27] and by theory[26,28], which established that α changes with quantum confinement and may even invert (become negative) in strongly confined II–VI quantum dots (although this has never yet been observed). This effect results from an admixture of *p*-type valence band states into the electron's Bloch wavefunction, causing a negative kinetic-exchange contribution to α that increases with confinement energy (β remains largely unaffected, being already dominated by kinetic exchange).

Following the work of Merkulov *et al.*[26], in quantum-confined systems α can be approximated as $\alpha = \alpha_{bulk} + |C_v|^2\gamma(E)\beta_{bulk}$, where the coefficient $|C_v|^2 \sim \Delta E_e/E_g$ describes the valence-band contribution to the electron's Bloch wavefunction, which scales as the ratio of the electron confinement energy, ΔE_e, to the bulk bandgap E_g. The kinetic-exchange parameter $\gamma(E)$ is calculated in second-order perturbation theory and depends strongly (resonantly) on the proximity of the confined electron and hole energies (E_e, E_h) to the occupied and unoccupied levels of the Mn^{2+} 3*d* electrons (ε^+, ε^-): $\gamma(E) = (E_h - \varepsilon^+)(\varepsilon^- - E_h)/(E_e - \varepsilon^+)(\varepsilon^- - E_e)$ (see Fig. 4c). Strong confinement in ZnSe nanocrystals influences $\gamma(E)$ primarily through the resonant $(\varepsilon^- - E_e)^{-1}$ term, because E_e shifts much closer to ε^- than in the bulk. Using literature values[29] (ε^+ is ~3.5 eV below the valence band edge and ε^- is ~3.5–4.0 eV above it), we estimate that α inverts sign (becomes negative) when $\Delta E_e > 200$–300 meV. In our 17-Å-radius ZnSe cores, the 1S absorption edge blueshifts by ~400 meV with respect to bulk ZnSe (see Fig. 1), indicating that $N_0\alpha$ is probably negative and of order −0.2 eV.

However, without a significant disparity between the carrier–Mn^{2+} overlap integrals $f_{e,h}$, a small negative value of α alone will not invert ΔE_Z. In nanocrystals with thin CdSe shells, $\Psi_e(\mathbf{r})$ and $\Psi_h(\mathbf{r})$ reside primarily in the core, so that $f_e \approx f_h$ and ΔE_Z remains dominated by the large hole–Mn^{2+} coupling and is negative, as experimentally observed (Fig. 2c). Inverting ΔE_z requires a marked and preferential reduction of hole–Mn^{2+} overlap, such that $f_h \ll f_e$. Precisely this situation occurs in nanocrystals with thicker CdSe shells ($h > \sim 2$ Å), where $\Psi_h(\mathbf{r})$ migrates to the non-magnetic shell more rapidly than $\Psi_e(\mathbf{r})$ (see Fig. 1), effectively 'turning off' the hole–Mn^{2+} coupling. Although not expected to occur in a model of S-like envelope wavefunctions alone[7], this disparity between f_e and f_h arises because, unlike $\Psi_e(\mathbf{r})$, $\Psi_h(\mathbf{r})$ has both S- and D-like spatial symmetry[24] (its radial wavefunction has both j_0 and j_2 spherical Bessel components; the latter vanishes at the nanocrystal centre and concentrates near the nanocrystal surface even in core-only nanocrystals). The relative contribution from j_2 increases with *h* because thicker shells favour localization of holes with D-type symmetry. Thus, f_h rapidly decreases to zero with increasing shell thickness, suppressing *p–d* exchange and inverting the *sp–d* exchange, $N_0(f_e\alpha - f_h\beta)$, as experimentally measured. Figure 4a,b explicitly illustrates how the relevant energy levels evolve with increasing *h*, in both an exciton ($\pm 1^U$) and in a separate electron–hole ($\mathbf{s}_e$, $\mathbf{j}_h$) picture (see figure caption for details). As demonstrated here, the extremely strong 'zero-dimensional' quantum confinement afforded in heterostructured nanocrystals leads to new regimes of tunable carrier–Mn^{2+} spin exchange in these materials, and future measurements are aimed at resolving, separately, the electron and hole exchange parameters.

Methods

Core–shell nanocrystal synthesis and characterization. Growth of the Mn^{2+}-doped, $r \cong 17$ Å ZnSe cores followed the procedure described in ref. 14. Overcoating with CdSe followed ref. 7, where 5 ml of ZnSe nanocrystals in hexadecylamine were transferred to 8 ml of dry trioctylphosphine oxide (TOPO) at 140 °C under nitrogen flow. Then, a mixture of 4 ml TOP, 0.25 ml 2 M TOPSe and 30 µl dimethylcadmium ($CdMe_2$) was slowly injected into the reaction. The temperature was gradually increased to 200 °C over 3–4 days while 4–5 extra injections of the TOP, TOPSe and $CdMe_2$ mixture were conducted. Photoluminescence and absorption spectroscopy were used to monitor the growth of the CdSe shell. To quench the reaction, the temperature was lowered to 100 °C and the sample was quickly mixed with hexane. Core and (thick) shell dimensions were directly measured by transmission electron microscopy. The Mn^{2+} concentration from elemental analysis of pyridine-washed Mn^{2+}-doped ZnSe cores was determined by inductively coupled plasma—optical emission spectroscopy to be ~0.4% ± 0.1% of all cations, corresponding to ~2 Mn^{2+} ions per ZnSe core, on average.

MCD measurements. MCD measures the normalized difference between the transmission of right- and left-circularly polarized light through the nanocrystal sample in the Faraday geometry, $(T_R - T_L)/(T_R + T_L)$, as a function of photon energy. When ΔE_Z is small compared with the Gaussian width, σ, of the fundamental 1S absorption peak, the MCD spectrum is derivative-like with a low-energy maximum amplitude I_{max} that is proportional to the Zeeman splitting: $\Delta E_Z = -2\sigma I_{max}/A_{max}$, where A_{max} is the absorbance of the nanocrystals at I_{max} (ref. 21). Low-temperature MCD studies were carried out on thin films of core–shell nanocrystals mounted in the variable temperature insert (1.5–300 K) of an 8 T superconducting magnet with direct optical access. Spectrally narrow (<0.5 nm) probe light of tunable wavelength was derived from a Xe lamp directed through a 0.3 m scanning spectrometer. Before being focused through the nanocrystal film, the probe beam was mechanically chopped at 137 Hz and its polarization was modulated between right- and left-circular at 84 kHz using a linear polarizer and a photoelastic modulator. A silicon avalanche photodiode detected the light transmitted through the sample, and $T_R - T_L$ and $T_R + T_L$ were extracted using lock-in amplifiers referenced to the photoelastic modulator and to the chopper, respectively.

Fitting to a Brillouin function. In the Mn^{2+}-doped nanocrystals, ΔE_Z is observed to saturate at low temperatures and high magnetic fields, tracking the average magnetization per Mn^{2+} ion, $\langle S_z \rangle$, which is defined as a negative quantity (antiparallel to **H**). To account for antiferromagnetic correlations and clustering among neighbouring Mn^{2+} ions, $\langle S_z \rangle$ is typically described by a modified Brillouin function, $\langle S_z \rangle = S_z^{sat} B_S[g_{Mn}\mu_B SH/k_B(T + T_0)]$, where $T + T_0$ is an effective temperature, $B_S(x) = ((2S+1)/2S)\coth[((2S+1)/2S)x] - (1/2S)\coth[(1/2S)x]$ is the Brillouin function and k_B is the Boltzmann constant. Mn^{2+} ions have total spin $\mathbf{S} = 5/2$. S_z^{sat} is the effective saturation value of $\langle S_z \rangle$ per Mn^{2+} ion, which may be considerably smaller than −5/2 when the average Mn^{2+} concentration $x_{Mn} > \sim 1\%$. At the low Mn^{2+} doping levels in these core–shell nanocrystals, the Mn^{2+} ions are largely isolated paramagnets. However, some Mn–Mn correlations are revealed by the non-zero fitting values of T_0 (for example, in Fig. 2, where the increase in $T + T_0$ from 4 to 9 K suggests extra Mn diffusion—and increased Mn–Mn interactions—during the 3–4 days required to grow thick CdSe shells).

Received 19 June 2008; accepted 12 November 2008; published online 14 December 2008

References

1. Ohno, H. *et al.* Electric-field control of ferromagnetism. *Nature* **408**, 944–946 (2000).
2. Zutic, I., Fabian, J. & Das Sarma, S. Spintronics: Fundamentals and applications. *Rev. Mod. Phys.* **76**, 323–410 (2004).
3. Furdyna, J. K. Diluted magnetic semiconductors. *J. Appl. Phys.* **64**, R29–R64 (1988).
4. Awschalom, D. D. & Samarth, N. Spin dynamics and quantum transport in magnetic semiconductor quantum structures. *J. Magn. Magn. Mater.* **200**, 130–147 (1999).
5. Kossut, J. Low-dimensional structures of diluted magnetic (semimagnetic) semiconductors—a subjective review. *Acta Phys. Pol. A* **100**, 111–138 (2001).
6. Kim, S., Fisher, B., Eisler, H. J. & Bawendi, M. Type-II quantum dots: CdTe/CdSe(core/shell) and CdSe/ZnTe(core/shell) heterostructures. *J. Am. Chem. Soc.* **125**, 11466–11467 (2003).
7. Balet, L. P. *et al.* Inverted core/shell nanocrystals continuously tunable between type-I and type-II localization regimes. *Nano Lett.* **4**, 1485–1488 (2004).
8. Bacher, G. *et al.* Optical spectroscopy on individual CdSe/ZnMnSe quantum dots. *Appl. Phys. Lett.* **79**, 524–527 (2001).
9. Kratzert, P. R., Puls, J., Rabe, M. & Henneberger, F. Growth and magneto-optical properties of sub 10 nm (Cd, Mn)Se quantum dots. *Appl. Phys. Lett.* **79**, 2814–2816 (2001).

10. Besombes, L. *et al.* Probing the spin state of a single magnetic ion in an individual quantum dot. *Phys. Rev. Lett.* **93**, 207403 (2004).
11. Bhargava, R. N., Gallagher, D., Hong, X. & Nurmikko, A. Optical properties of manganese-doped nanocrystals of ZnS. *Phys. Rev. Lett.* **72**, 416–419 (1994).
12. Hoffman, D. M. *et al.* Giant internal magnetic fields in Mn doped nanocrystal quantum dots. *Solid State Commun.* **114**, 547–550 (2000).
13. Radovanovic, P. V. & Gamelin, D. R. Electronic absorption spectroscopy of cobalt ions in diluted magnetic semiconductor quantum dots: Demonstration of an isocrystalline core/shell synthetic method. *J. Am. Chem. Soc.* **123**, 12207–12214 (2001).
14. Norris, D. J., Yao, N., Charnock, F. T. & Kennedy, T. A. High-quality manganese-doped ZnSe nanocrystals. *Nano Lett.* **1**, 3–7 (2001).
15. Archer, P. I., Santangelo, S. A. & Gamelin, D. R. Direct observation of sp–d exchange interactions in colloidal Mn^{2+}- and Co^{2+}-doped CdSe quantum dots. *Nano Lett.* **7**, 1037–1043 (2007).
16. Norris, D. J., Efros, Al. L. & Erwin, S. C. Doped nanocrystals. *Science* **319**, 1776–1779 (2008).
17. Bhattacharjee, A. K. & Perez-Conde, J. Optical properties of paramagnetic ion-doped semiconductor nanocrystals. *Phys. Rev. B* **68**, 045303 (2003).
18. Archer, P. I., Santangelo, S. A. & Gamelin, D. R. Inorganic cluster syntheses of TM^{2+}-doped quantum dots (CdSe, CdS, CdSe/CdS): Physical property dependence on dopant locale. *J. Am. Chem. Soc.* **129**, 9808–9818 (2007).
19. Erwin, S. C. *et al.* Doping semiconductor nanocrystals. *Nature* **436**, 91–94 (2005).
20. Beaulac, R. *et al.* Spin-polarizable excitonic luminescence in colloidal Mn^{2+}-doped CdSe quantum dots. *Nano Lett.* **8**, 1197–1201 (2008).
21. Kuno, M. *et al.* Magnetic circular dichroism study of CdSe quantum dots. *J. Chem. Phys.* **108**, 4242–4247 (1998).
22. Myers, R. C. *et al.* Optoelectronic control of spin dynamics at near-terahertz frequencies in magnetically doped quantum wells. *Phys. Rev. B* **72**, 041302 (2005).
23. Gaj, J. A. in *Diluted Magnetic Semiconductors* Vol. 25 (eds Furdyna, J. K. & Kossut, J.) 275–309 (Academic, 1988).
24. Efros, Al. L. *et al.* Band-edge exciton in quantum dots of semiconductors with a degenerate valence band: Dark and bright exciton states. *Phys. Rev. B* **54**, 4843–4856 (1996).
25. Mackh, G., Ossau, W., Waag, A. & Landwehr, G. Effect of the reduction of dimensionality on the exchange parameters in semimagnetic semiconductors. *Phys. Rev. B* **54**, R5227–R5230 (1996).
26. Merkulov, I. A. *et al.* Kinetic exchange between the conduction band electrons and magnetic ions in quantum-confined structures. *Phys. Rev. Lett.* **83**, 1431–1434 (1999).
27. Myers, R. C. *et al.* Antiferromagnetic s–d exchange coupling in GaMnAs. *Phys. Rev. Lett.* **95**, 017204 (2005).
28. Bhattacharjee, A. K. Confinement-induced reduction of the effective exchange parameters in semimagnetic semiconductor nanostructures. *Phys. Rev. B* **58**, 15660–15665 (1998).
29. Larson, B. E. & Ehrenreich, H. Anisotropic superexchange and spin-resonance linewidth in diluted magnetic semiconductors. *Phys. Rev. B* **39**, 1747–1759 (1989).

Acknowledgements

We thank B. Prall for technical assistance. This work was supported by Los Alamos LDRD Funds and the Chemical Sciences, Biosciences, and Geosciences Division of the Office of Basic Energy Sciences, Office of Science, US Department of Energy (DOE). D.A.B. and V.I.K. are partially supported by the DOE Center for Integrated Nanotechnologies jointly operated by Los Alamos and Sandia National Laboratories. A.L.E. acknowledges financial support from ONR.

Additional information

Supplementary Information accompanies this paper on www.nature.com/naturematerials. Reprints and permissions information is available online at http://npg.nature.com/reprintsandpermissions. Correspondence and requests for materials should be addressed to S.A.C. or V.I.K.